Journal of Fluids and Structures 18 (2003) 347–366

JOURNAL OF FLUIDS AND STRUCTURES

www.elsevier.nl/locate/jnlabr/yjfls

Reduction of fluid forces acting on a single circular cylinder and two circular cylinders by using tripping rods

Md. Mahbub Alam, H. Sakamoto*, M. Moriya

Department of Mechanical Engineering, Kitami Institute of Technology, 165 Koen-cho, Kitami, Hokkaido 090-8507, Japan

Received 3 July 2002; accepted 20 July 2003

Abstract

The effects of tripping rods on flow characteristics and fluid forces acting on a single cylinder and on two cylinders in side-by-side and tandem arrangements were investigated in a smooth cross stream at a Reynolds number of 5.5×10^4. At first, tripping rods of 4, 5 and 6 mm in diameter were used on a single cylinder of diameter 49 mm. The angular position of the tripping rods was varied from 20° to 60°. The optimum angular position of tripping rods for reducing fluid forces was found to be 30°. Two tripping rods, each of 5 mm in diameter, positioned symmetrically at this angle reduced steady drag, fluctuating drag and fluctuating lift forces acting on the cylinder by 67%, 61% and 87%, respectively. A bistable nature of the flow on the single cylinder appears when the tripping rods were positioned at 41°–44°. Next, fluid forces acting on two circular cylinders in a side-by-side or tandem arrangement were reduced by using tripping rods on both cylinders. A significant reduction in both steady and fluctuating fluid forces acting on the side-by-side cylinders was observed when the gap spacing between the cylinders was greater than the diameter of a cylinder. In the case of tandem cylinders with tripping rods, fluid forces acting on the upstream cylinder were almost independent on the downstream cylinder at any spacing of the cylinders. The critical spacing at which a bistable flow appears was found at spacing ratios of 3.0 and 2.6 for the plain cylinders and the cylinders with tripping rods, respectively. At the critical spacing, however, there was no considerable jump in fluid forces acting on the upstream cylinder when tripping rods were used on the cylinder. Wavelet analysis was used to study the bistable flow for the single cylinder with tripping rods and for the tandem cylinders.

1. Introduction

When a fluid is in a relative motion past a stationary structure or a bluff body, the structure or the bluff body may experience both steady and fluctuating fluid forces. Structures are usually made sufficiently strong so that they can resist these forces. Therefore, the steady and fluctuating fluid forces acting on a structure or group of structures are major criteria for the design of structures. The structures on the earth's surface experience a turbulent boundary layer flow. This study, however, is concerned with a two-dimensional smooth flow, and the results obtained for a smooth flow can not be directly extrapolated to those for a turbulent boundary flow (Jendrzejczyk and Chen, 1982; Kareem et al., 1998). Reduction of fluid forces caused by motion of a fluid is now a major issue in many fields of engineering.

Many methods for reducing and suppressing fluid forces acting on a single structure have been proposed by Zdravkovich (1981). However, most structures on land and in the ocean have complex forms, and the action of flow past multiple structures is very complex and different from that on a single structure. Thus, it is comparatively difficult to reduce fluid forces acting on multiple structures. Alam et al. (2002) recently performed an experiment on reduction of fluid forces acting on two square cylinders in a tandem arrangement. To reduce fluid forces acting on the cylinders, a

*Corresponding author. Tel./fax: +81-157-26-9207.
E-mail address: sakamoto@mech.kitami-it.ac.jp (H. Sakamoto).

0889-9746/$ - see front matter
doi:10.1016/j.jfluidstructs.2003.07.011

thin flat plate was positioned centrally in front of the upstream cylinder. They found that the fluid forces acting on both cylinders decreased dramatically when the control plate was placed in front of the upstream cylinder at a distance of 1.50–1.90 times the width of the cylinder.

Tandem and side-by-side arrangements of two circular cylinders are simple cases of an array of multiple structures (Fig. 1). The mutual interference effect of two cylinders is very strong in tandem arrangement (Hori, 1959), and this effect results in a significant change in fluid forces acting on the cylinders depending on the spacing between them (Zdravkovich and Pridden, 1977; Okajima, 1979; Igarashi, 1984; Alam et al., 2003b). In the case of two cylinders in a tandem arrangement, there is a critical spacing at which fluid forces acting on the cylinders jump from a low value to a high value and then intermittently switch between those values (Zdravkovich and Pridden, 1977; Okajima, 1979; Kiya et al., 1980; Igarashi, 1984; Jendrzejczyk and Chen, 1986; Zhang and Melbourne, 1992). This phenomenon is known as the jump phenomenon, and it is caused by the occurrence of a bistable flow, which excites interference-induced oscillations [see Chen (1986) and Zdravkovich (1988) for reviews]. Studies on two cylinders in various arrangements have been reviewed by Zdravkovich (1977). Alam et al. (2003b) reported that fluctuating fluid forces acting on the downstream cylinder of two cylinders in a tandem arrangement were of a large magnitude not only at the critical spacing but also at the spacing of $L/D = 1.40$ (see Fig. 1 for definition of the symbols). At this spacing, the shear layer that separated from the upstream cylinder reattached alternately with a smaller angle of incidence to the downstream

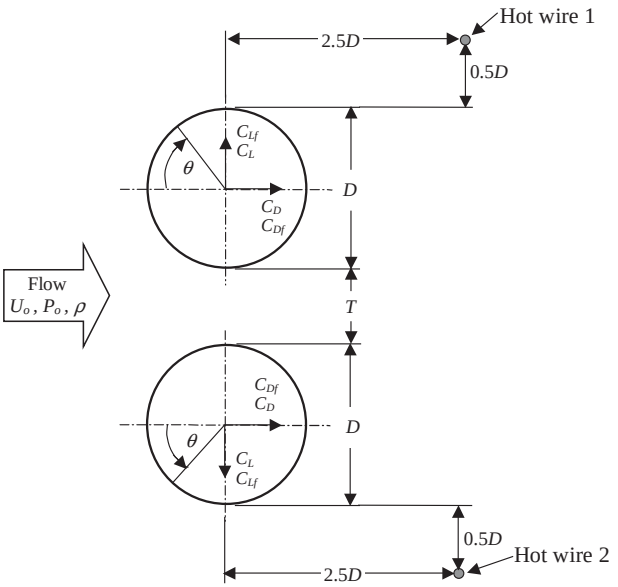

(a) Side-by-side arrangement

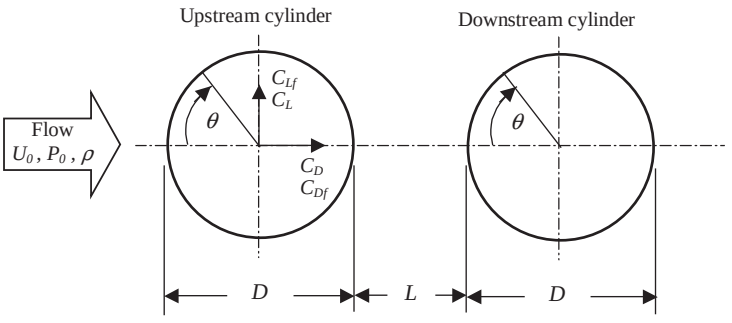

(b) Tandem arrangement

Fig. 1. Sketch of the coordinate system and hotwire positions.

cylinder. Considering the above points, it is important to establish a method for reducing bistable flow and fluid forces acting on two circular cylinders in tandem as well as side-by-side arrangement.

Steady fluid forces acting on two side-by-side cylinders have been measured by Biermann and Herrnstein (1933), Hori (1959), Bearman and Wadcock (1973), Zdravkovich and Pridden (1977), and Jendrzejczyk and Chen (1982); however, there have been few studies pertaining to fluctuating fluid forces. As the spacing between two side-by-side cylinders is varied, two major flow regimes, characterized by the behavior of the wake region, are observed. In the first regime of flow, which is known as a bistable flow regime (Bearman and Wadcock, 1973; Kim and Durbin, 1988), the wake behind the cylinders is grossly unsteady and asymmetric and the gap flow is biased toward one side or the other; consequently, the cylinder toward which the flow is biased has a narrower near wake (designated mode 'NW' in this paper, see Fig. 2), while the other cylinder has a wider near wake (designated mode 'WW'). Mode 'NW' pertains to relatively strong drag force and high vortex shedding frequency, and mode 'WW' pertains to relatively weak drag force and low vortex shedding frequency. In the second regime of flow, the wake behind one cylinder is similar to that behind the other, and the wakes behind the two cylinders exhibit the same frequencies. It is known that two side-by-side cylinders may be subjected to vibration and/or instability (Mahir and Rockwell, 1996; Zhou et al., 2001). Determination of fluid forces acting on two stationary cylinders in groups is essential for assessment of structural response. Considering the practical environment of landbase structures, an experimental investigation on the interference effect between two and three cylinders of finite height immersed in a turbulent boundary layer was performed by Kareem et al. (1998).

The use of tripping rods to reduce drag as well as to change the characteristics of flow over a cylinder is very interesting. A basic study on the effects of tripping rods was carried out by Fage and Warsap (1929), who placed two small tripping rods on the surface of a cylinder at $\pm 65^\circ$ and measured the drag force in the transition range of the Reynolds number. However, they did not study effects of different positions of the tripping rods. The mechanism of reducing drag by using tripping rods is that the tripping rods alter a subcritical flow into a natural transition flow or into a critical flow. However, the alteration of a higher subcritical flow over a cylinder into a transition flow (or transcritical flow) can also be achieved by increasing the roughness of the cylinder and/or by increasing the free-stream turbulent intensity. In the case of a lower subcritical Reynolds number flow with small turbulent intensity, use of tripping rods to change the subcritical flow into a transition flow is very effective. The effects of various diameters and locations of tripping rods on the flow over a cylinder were studied by James and Truong (1972) and Igarashi (1986). James and Truong conducted experiments in the range of Reynolds numbers of 10^4–10^5 using tripping rods with diameters of 0.6–6.3% of the cylinder diameter. Their data showed that larger tripping rods caused transition at an earlier Reynolds number and that the optimum location of tripping rods also shifted toward the stagnation point with an increase in tripping rod diameter. For example, for tripping rods with diameters of 0.6% and 6.3% of the cylinder diameter, the optimum locations were found to be at 65° and 35°, respectively. Pearcey et al. (1982) reported that the diameters of the tripping rods must be quite large to modify a very low Reynolds number flow to a critical flow. The effects of tripping rods with large diameter on the characteristics of flow as well as on pressure distribution, Strouhal number, steady drag and lift forces were studied by Nebres and Batill (1993). They used tripping rods with diameters of 0.7–14% of the cylinder diameter, and angular positions of the tripping rods were varied in the entire domain. They found that tripping rod had no effect on the flow characteristics when it was positioned near either the stagnation region or base region but that the tripping rod has a considerable effect on flow characteristics at an angular position of 20°–70° and that the optimum location of a tripping rod for reducing fluid forces acting on a cylinder depends on the tripping rod diameter and the Reynolds number. The studies described above focused on the effects of tripping rods on steady fluid forces. There have been few studies, however, in which the effects of tripping rods on fluctuating fluid forces acting on a cylinder or multiple cylinders were investigated. In the present study, therefore, we investigated both steady and fluctuating fluid forces acting on a single cylinder and on two cylinders in side-by-side and tandem arrangements. Romberg and Popp (1998) and Hover et al. (2001) investigated the effects of tripping rods on the flow-induced instability of a single cylinder and one cylinder in a bundle, respectively. The studies discussed above are concerned with

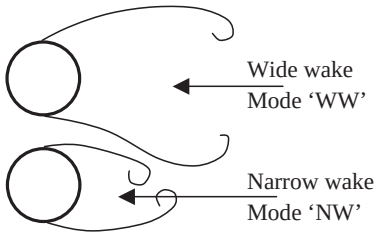

Fig. 2. Schematic illustration of an asymmetric wake structure.

using one or two tripping rods placed symmetrically along the span of a cylinder. Naumann and Quadflieg (1972) and Kareem and Cheng (1999) examined flow patterns and spatio-temporal pressure fluctuations on a cylinder when an additional pair of rods was used on the rear surface where the final separation of the shear layer occurs.

The first objective of the present study was to determine in more detail the structure of a flow around a cylinder with tripping rods and to determine the optimum location of tripping rods for reducing fluid forces. The second objective was to determine how the action of a bistable flow can be reduced and how fluid forces acting on two cylinders in side-by-side and tandem arrangements can be reduced. Measurements were carried out systematically in the range of spacing $T/D, L/D = 0.1-5$ (see Fig. 1 for definition of symbols). Tests were carried out with and without tripping rods so as to elucidate the effects of the tripping rods. The results are discussed on the basis of results of wavelet analysis, surface pressure distribution, vortex shedding frequency, and surface oil-flow patterns.

2. Experimental arrangement and procedures

Experiments were carried out in a low-speed, closed-circuit wind tunnel. The test section of the wind tunnel was rectangular with a height of 1.2 m, width of 0.3 m and length of 2.5 m. The cylinders used as test models each had a diameter of 49 mm and length of 0.4 m. The cylinders spanned the horizontal 0.3-m dimension of the tunnel. For all measurements, the free-stream velocity, U, in the tunnel was kept constant at 17 m/s. A honeycomb was placed at the entrance of the test section to produce a uniform flow. To corroborate that the flow in the test-section was uniform, a calibrated hotwire was traversed across the whole test section of the tunnel. Within the middle 0.24×0.95 m of the test-section, the flow was uniform within $\pm 2\%$ of the center-line velocity. In the same region, the turbulence intensity was also uniform and less than 0.5% of the free-stream velocity. The geometric blockage ratio and aspect ratio at the test section were 4% and 6, respectively, based on a single cylinder.

Fig. 3(a) shows a symmetrical arrangement of two tripping rods on a cylinder and the coordinate system. In this figure, α is the angular position of a tripping rod, δ is the gap between a tripping rod and the cylinder, and θ is the angular position of a point on the surface of the cylinder. Tripping rods with diameters of 4, 5 and 6 mm were used in this study. Several pairs of square blocks, as shown in Fig. 3(b), were used to hold the tripping rods and the cylinder to the tunnel wall. A number of holes at different angular positions on a circle with $\delta = 0.40$ mm were made in the blocks, so that the tripping rods could be placed precisely at the desired position. The diameters of the holes for the tripping rods were the same as the diameters of the tripping rods, and each hole was 35 mm in length. As a result, fluid forces acting on the tripping rods did not cause any vibration or rotation of the tripping rods.

Fluid forces acting on a cylinder were measured by using two load cells installed inside a cylinder as shown in Fig. 4. The load cell inside the active cylinder measured a combination of fluid forces and forces due to vibration transmitted from the outside through the cylinder support. The other load cell was installed inside the dummy cylinder to measure forces due to vibration transmitted from the outside through the cylinder support. Hence, the fluid forces acting on the active cylinder could be calculated by subtracting the output of the load cell installed inside the dummy cylinder from that of the load cell installed inside the active cylinder. The details of load cells and procedure for measuring fluid forces have been described in detail by Sakamoto et al. (1994). The sensitivity of the load cells was 11.311 mV/g.

A semiconductor pressure transducer (Toyoda PD104K) with a range of ± 10 kPa was used to measure the surface pressure during experiments. The transducer output was calibrated to give a reading of 6.22 V for 1 kPa of applied pressure. The pressure transducer responded to pressure fluctuation up to 500 Hz with a gain factor of 1 ± 0.06, the phase lag being negligible.

Surface oil-film techniques were used to confirm the flow pattern on the cylinders. The cylinders were wrapped with a black film of 0.03 mm in thickness, and then an even coating of a solution containing silicone oil, titanium dioxide, oleic acid and kerosene at a ratio of 45:3:2:2 in weight was applied to the surface. The solution distribution on the cylinder surface was achieved after at least 15 min of exposure to the uniform flow in the wind tunnel. Finally, the black film was unwrapped carefully, and photographs of solution distribution on the film were taken with a digital camera.

3. Results and discussion

3.1. Tripping rods on a single cylinder

3.1.1. Effects of tripping rods on fluid forces and flow characteristics

First the effect of the gap, δ, on fluid forces acting on a single cylinder was investigated for tripping rods with a diameter of 5 mm placed at an angular position of $\alpha = 30^\circ$. Measurements of drag coefficient, C_D, fluctuating drag

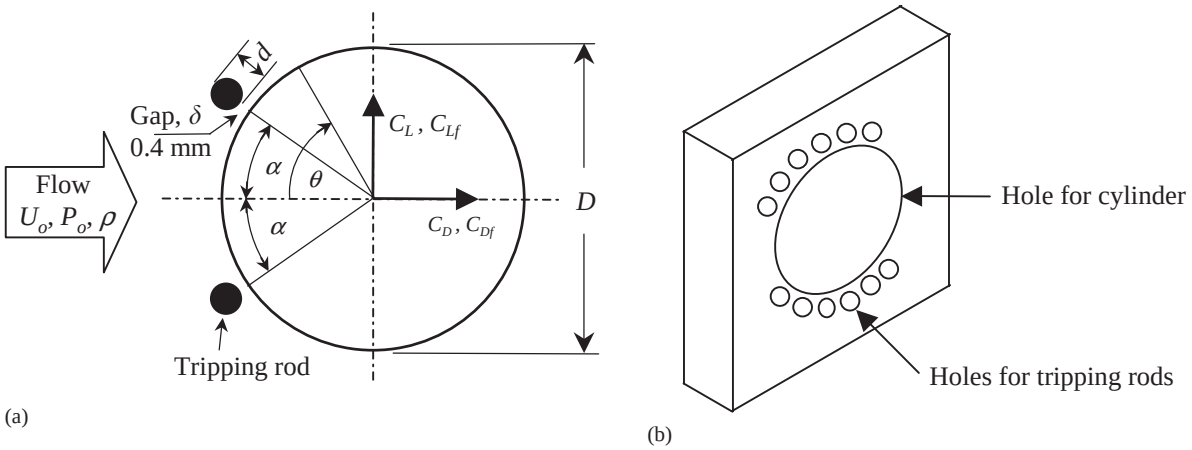

Fig. 3. (a) Arrangement of tripping rods and definitions of symbols, (b) block for holding cylinder and tripping rods.

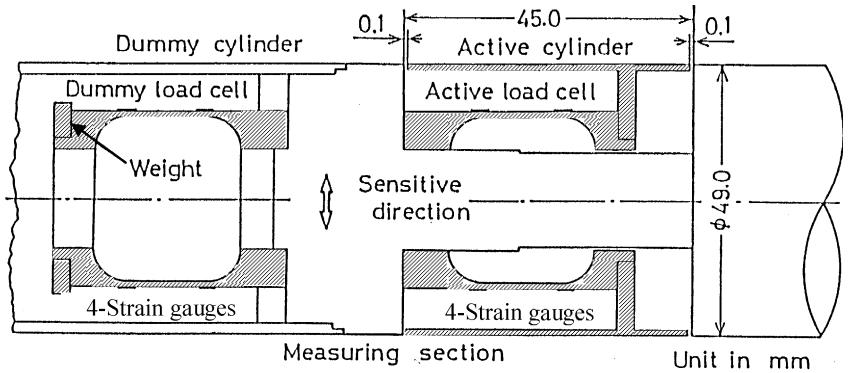

Fig. 4. Arrangement of load cells inside a cylinder.

coefficient, C_{Df}, and fluctuating lift coefficient, C_{Lf}, as a function of gap ratio, δ/D, are shown in Fig. 5. Note that all measurements were carried out at a subcritical Reynolds number of 5.5×10^4. The gap ratio was varied from $\delta/D =$ 0.008 to 0.22 ($\delta = 0.4-12$ mm). Measurements at $\delta/D = 0$ (i.e., tripping rods in contact with the cylinder) were not possible in our experiment because a clearance between the tripping rod and the cylinder was necessary to measure the fluid forces using the load cells. It can be seen in Fig. 5 that fluid force coefficients are almost independent of the gap ratio for $\delta/D < 0.15$. It is noted that the diameters of the tripping rods are greater than the boundary layer thickness at $\theta = 30^\circ$. The boundary layer thickness at $\theta = 30^\circ$ on a plain cylinder (a cylinder without tripping rods), which was calculated by the approximation method of Pohlhausen (1921), is 0.25 mm. This value agrees well with that measured by Nebres and Batill (1993).

For all subsequent measurements, the gap was maintained at 0.4 mm. The effects of tripping rod position, α, on C_D, C_{Df} and C_{Lf} in the case of the tripping rods with diameters of 4, 5, and 6 mm are shown in Fig. 6. Fig. 6(a) shows that C_D is a minimum for rod placement at $\alpha = 30^\circ$. At this position of tripping rods, C_D is reduced by 67% in the case of tripping rods with diameters of 5 mm. Note that the values of C_D, C_{Df} and C_{Lf} for a plain cylinder are 1.12, 0.14 and 0.48, respectively. These values are similar to those measured by Bearman (1969), Lesage and Gartshore (1987), Szepessy and Bearman (1992), Nebres and Batill (1993), Sakamoto et al. (1994), and West and Apelt (1997). The value of C_D for $\alpha = 45^\circ - 60^\circ$ exceeds the value of the plain cylinder. It is interesting that C_{Df} and C_{Lf} (Fig. 6(b,c)) are greatly reduced for a wide range of tripping rod positions (30°–40°). In this range of tripping rod positions, C_{Df} and C_{Lf} are reduced by 61% and 87%, respectively, in the case of tripping rods with diameters of 5 mm. At $\alpha = 60^\circ$, the values of C_{Df} and C_{Lf} are much larger than those of a plain cylinder. The ranges $\alpha < 20^\circ$ and $\alpha > 60^\circ$ were not investigated since it was thought that these ranges of tripping rod positions would have little effect on the flow (Pearcey et al., 1982; Nebres and Batill, 1993). The variations in C_D, C_{Df} and C_{Lf} in Fig. 6(a–c) indicate that three regimes of force coefficients pertain to three kinds of flow patterns when α is varied from 20° to 60°. One regime, $\alpha = 20^\circ - 40^\circ$, is a reattachment

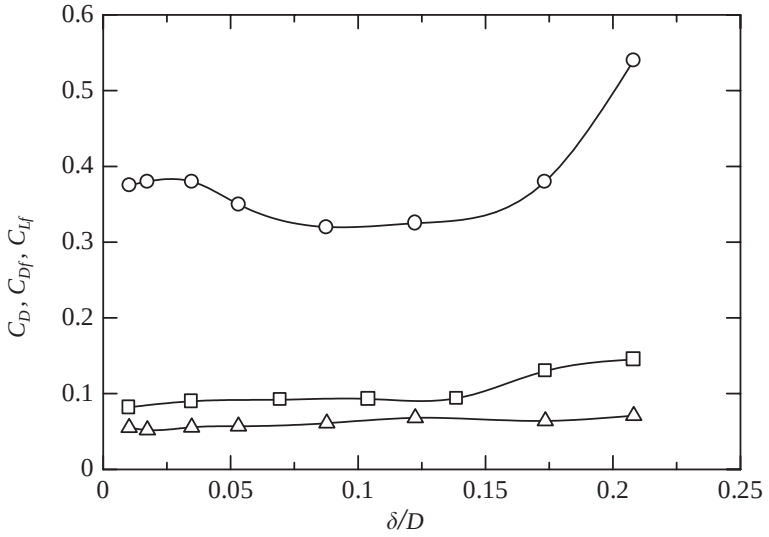

Fig. 5. Effect of gap ratio, δ/D, on force coefficients: ○, C_D; △, C_{Df}; □, C_{Lf}.

flow (hereafter defined as pattern A) in which the boundary layers separate from the tripping rods and reattach on the surface of the cylinder behind the tripping rods. A surface oil-film technique was used to confirm the reattachment of boundary layers. Typical surface oil-flow patterns and corresponding sketches of flow patterns for $\alpha = 30^\circ, 40^\circ$ and 60° are shown in Fig. 7. The surface oil-flow pattern (Fig. 7(a)) shows that the boundary layers separate from the tripping rods and reattach on the cylinder surface behind the tripping rods at $\theta = \pm 52^\circ$ and that this is followed by laminar separation at $\theta = \pm 87^\circ$. The oil-flow pattern for $\alpha = 40^\circ$ (Fig. 7(b)) is qualitatively the same as that for $\alpha = 30^\circ$. In this case, reattachment of the boundary layers occurs at $\theta = \pm 64^\circ$, and this is followed by laminar separation at $\theta = \pm 89^\circ$. Another regime, $\alpha = 45^\circ - 60^\circ$, is a separated flow (hereafter defined as pattern B) in which boundary layers separate from the cylinder at a position sufficiently upstream of the tripping rods, and the tripping rods force the separated boundary layer to deflect outside as shown in Fig. 7(c). Consequently, stronger wake vortices are generated for this range of α. The figure shows that the boundary layer separates from the cylinder surface at $\theta = \pm 46^\circ$ for $\alpha = 60^\circ$. The third regime, $\alpha = 41^\circ - 44^\circ$, is a bistable flow (hereafter defined as pattern C) in which two flow patterns (A and B) appear intermittently.

Fig. 8 presents the time-averaged pressure coefficient, C_P, and the fluctuating pressure coefficient, C_{Pf}, around a cylinder with tripping rods 5 mm in diameter at different angular positions. Those of a plain cylinder are also shown for comparison. The most obvious effect is a drastic change in pressure across the tripping rods. In Fig. 8(a), the magnitudes of C_P in the base region for $\alpha = 30^\circ$ and 40° are considerably smaller than those of the plain cylinder, while C_P for $\alpha = 60^\circ$ is considerably higher. It is notable that there are peaks in the C_P distribution at $\theta = \pm 60^\circ$ ($-60^\circ = 300^\circ$) and $\pm 70^\circ$ ($-70^\circ = 290^\circ$) for $\alpha = 30^\circ$ and 40°, respectively. These peaks are due to reattachments of boundary layers that have separated from the tripping rods. It was shown in the surface oil-flow patterns (Fig. 7(a,b)) that the boundary layers reattach at $\theta = \pm 52^\circ$ and $\pm 64^\circ$ for $\alpha = 30^\circ$ and 40°, respectively. Thus, the peaks are formed somewhat downstream of the reattachments. In a study on the flow behind a step by Mueller (1961), it was found that the maximum pressure recovery point corresponds to the point just a little after reattachment. The results for surface oil-flow pattern and pressure distributions in the present study agree with those of the study by Mueller. For $\alpha = 60^\circ$, a small adverse pressure gradient in the region of $\theta = \pm(40^\circ - 50^\circ)$ indicates separation of boundary layers at $\theta = \pm 46^\circ$ (Fig. 7(c)).

Fig. 8(b) shows that the value of C_{Pf} for $\alpha = 30^\circ$ and 40° is considerably smaller than that of the plain cylinder on the whole surface of the cylinder, while for $\alpha = 60^\circ$, the value of C_{Pf} in the region beyond the tripping rods is higher than that of the plain cylinder. Hence it can be inferred that the alternating Karman type vortex is almost suppressed at $\alpha = 30^\circ$ and 40° and that the Karman vortex is stronger at $\alpha = 60^\circ$.

3.1.2. Strouhal number

Fig. 9 shows the influence of angular position of the tripping rods on the Strouhal number, St, calculated from the results of spectral analysis of fluctuating lift force acting on the cylinder. As can be seen in the figure, the trend in

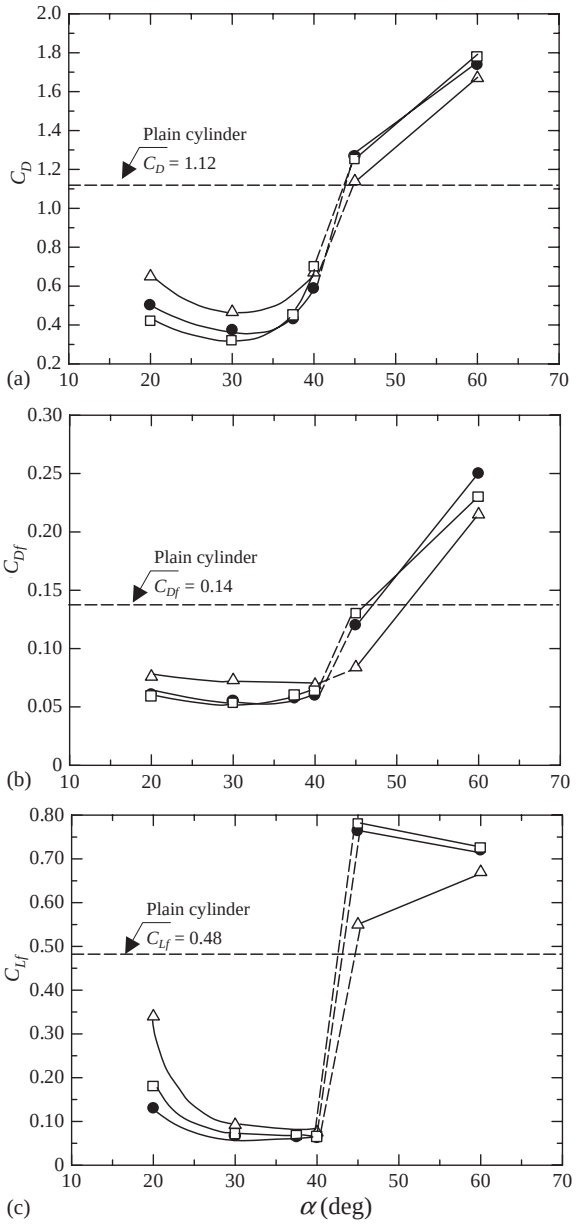

Fig. 6. Effect of angular position of tripping rods on force coefficients: (a) C_D, (b) C_{Df}, (c) C_{Lf}: △, $d/D = 0.08$ ($d = 4$ mm); ●, $d/D = 0.10$ ($d = 5$ mm); □, $d/D = 0.12$ ($d = 6$ mm).

Strouhal number variation is opposite to that of the drag coefficient with change in α. For $\alpha = 20^\circ - 40^\circ$ (pattern A), the Strouhal number is comparatively high and is maximum at $\alpha = 30^\circ$, indicating that the weakest vortex is formed at this position of tripping rods. For $\alpha = 45^\circ - 60^\circ$ (pattern B), the Strouhal number is lower than that of the plain cylinder. The Strouhal number suddenly decreases when α is changed from 40° to 45°. A sudden decrease in the Strouhal number in the same range of α for $d/D = 0.09$ was also found by Nebres and Batill (1993), but the cause of the sudden decrease was left unexplained in his study. It has been mentioned that flow patterns A and B appear intermittently for the range of tripping rod positions of $\alpha = 41^\circ - 44^\circ$ (pattern C). Thus, for $\alpha = 41^\circ - 44^\circ$, two peaks are sometimes found in the power spectrum as shown in Fig. 10. Considering the values of C_D, C_{Df}, C_{Lf}, and the Strouhal number, 30° can be regarded as the optimum angle of placement of the tripping rods of 5 mm in diameter for reducing fluid forces.

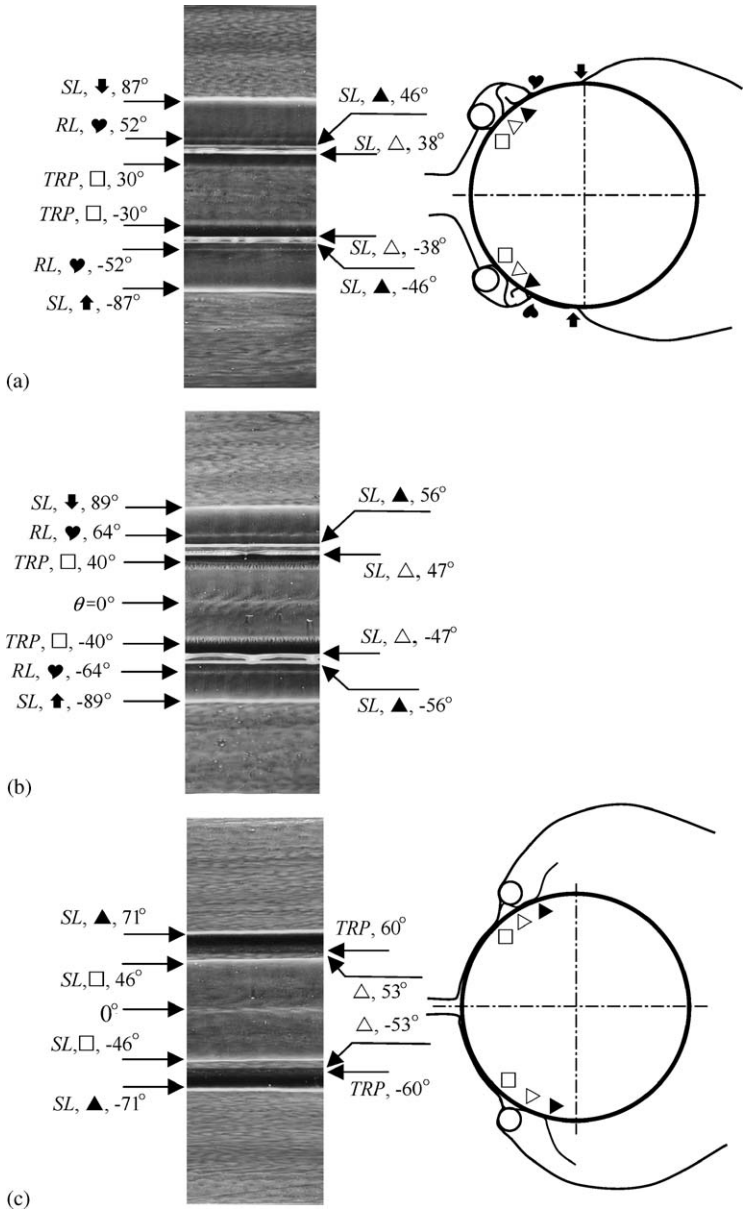

Fig. 7. Oil-flow patterns and corresponding sketch of flow patterns: (a) $\alpha = 30^\circ, d = 5\,\text{mm}$; (b) $\alpha = 40^\circ, d = 5\,\text{mm}$, definitions of symbols are the same as those in the sketch (a); (c) $\alpha = 60^\circ, d = 5\,\text{mm}$. *TRP*, tripping rod position; *RL*, reattachment line; *SL*, separation line.

Wavelet analysis can be used to examine the intermittent appearance of flow patterns A and B for $\alpha = 41^\circ - 44^\circ$. For a given one-dimensional function $u(t)$, the wavelet transform can be defined as

$$W(s,b) = p(s) \int u(t) \Psi^* \left(\frac{t-b}{s} \right) \mathrm{d}t, \tag{1}$$

where $W(s,b)$ is the wavelet coefficient, the superscript "$*$" denotes the complex conjugate, b is the translation parameter, s is the scale parameter. The function $\psi(t)$ is called an analyzing wavelet or mother wavelet. A well-known function such as the Morlet function or the Mexican hat function is often used as the mother wavelet. The Mexican hat function has a better time resolution property but a poorer frequency resolution property. The Morlet function, however, has a better frequency resolution property. A real-valued wavelet function such as the Mexican hat function

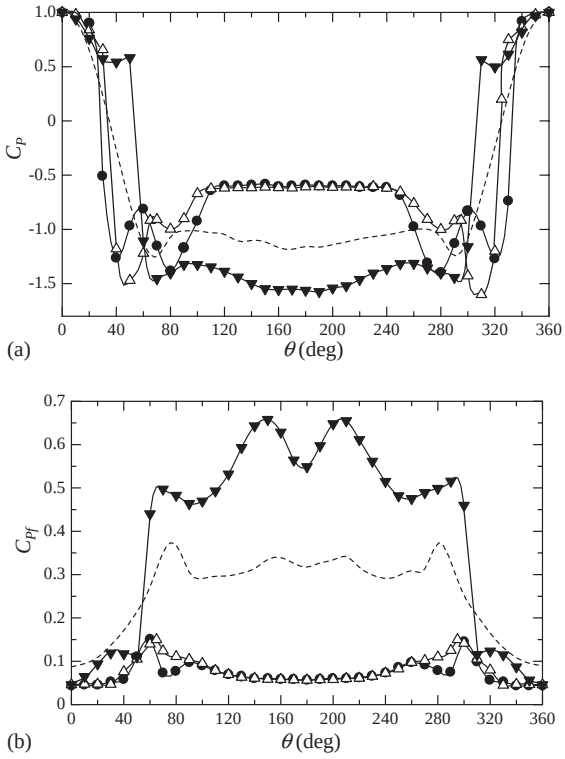

Fig. 8. Time-averaged and fluctuating pressure distributions ($d = 5$ mm): (a) time-averaged pressure, (b) fluctuating pressure: ----, plain cylinder; ●, $\alpha = 30^\circ$; △, $\alpha = 40^\circ$; ▼, $\alpha = 60^\circ$.

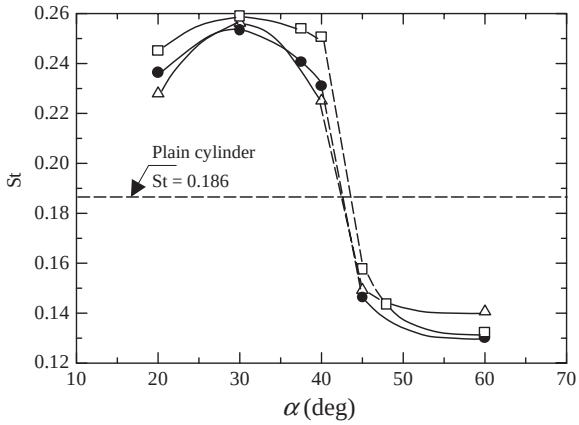

Fig. 9. Change in Strouhal number with change in angular position of tripping rod: △, $d/D = 0.08$ ($d = 4$ mm); ●, $d/D = 0.10$ ($d = 5$ mm); □, $d/D = 0.12$ ($d = 6$ mm).

can isolate peaks or discontinuities in terms of frequency and time (Lewalle, 1994). On the other hand, a complex-valued wavelet function such as the Morlet wavelet can trace out information on both amplitude and phase and is better adapted for capturing oscillatory behavior. In the present study, the Morlet function was used as a mother wavelet. This function is expressed as

$$\Psi(\eta) = e^{i\omega_0\eta} e^{-\eta^2/2}, \tag{2}$$

where ω_0 is the wave number in the Morlet wavelet. The larger the wave number, ω_0, the broader the wavelet power in time space. A narrower (in time) wavelet function has a good time resolution property but a poor frequency resolution

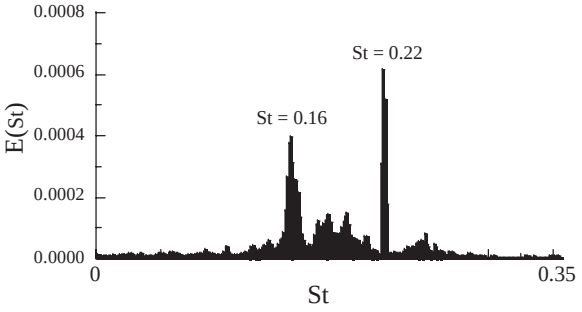

Fig. 10. Power spectrum of fluctuating lift: $d = 5\,\text{mm}$, $\alpha = 42^\circ$.

property, while a broad wavelet function has poor time resolution but good frequency resolution (Torrence and Compo, 1998). The Morlet wavelet with $\omega_0 = 6$ is marginally admissible. For the Morlet wavelet with wave number, ω_0, the relation between scales, s, and the Fourier frequency is

$$f = \frac{\omega_0 + \sqrt{2 + \omega_0^2}}{4\pi s}. \tag{3}$$

In Eq. (1), $p(s)$ is a weighting function that can be chosen as $s^{-1}, s^{-0.5}, s^{0.5}$ or s^0 depending on what we want to extract from the signal (Lewalle, 1994; Farge, 1992; Hamdan et al., 1996; Arneodo et al., 1988). The weighting function $p(s) = s^{-0.5}$ provides the same energy at each scale. However, a more negative power of s, such as s^{-1}, provides energy magnification at higher frequencies (lower scale), and nonnegative powers of s, such as s^0 or $s^{0.5}$, provide energy magnification at lower frequencies (higher scale).

Fig. 11 shows the wavelet power spectra (Eq. (1)) of a signal of fluctuating lift of the cylinder with tripping rods of 5 mm in diameter and positioned at an angle of 42° (pattern C). Fig. 11(a) shows a power spectrum for $p(s) = s^{-0.5}$, which ensure the same energy at each scale; that is, the local energy at any scale is governed by the amplitude of the signal. The figure implies that there are two frequencies in the lift signal, with Strouhal numbers of about 0.22 and 0.16. It can also be seen in the figure that energy at the higher Strouhal number is lower than that of the lower Strouhal number. These results agree with those shown in Figs. 6 and 9. Those figures showed that, for $\alpha = 40^\circ$, there was a higher Strouhal number and a lower fluctuation in the lift force acting on the cylinder (pattern A), and for $\alpha = 45^\circ$, there was a lower Strouhal number and a higher fluctuation in the lift force acting on the cylinder (pattern B). Therefore, in Fig. 11(a), the higher Strouhal number with lower energy corresponds to pattern A, and the lower Strouhal number with higher energy corresponds to pattern B. In order to highlight the energy at the higher Strouhal number in Fig. 11(a), the weighting function was changed to $p(s) = s^{-1.5}$, and the results are shown in Fig. 11(b). Here the higher Strouhal number is clearer. It is also clear that higher and lower Strouhal numbers appear intermittently. This implies that flow patterns A and B appear intermittently for $\alpha = 42^\circ$. Figs. 11(c) and (d) each show a global wavelet power spectrum (the marginal wavelet power spectrum) (Torrence and Compo, 1998) defined as

$$\overline{W^2}(s) = \int_{-\infty}^{\infty} |W(s,b)|^2 \, \mathrm{d}b, \tag{4}$$

which gives total energy at each scale. Two peaks at the dominating Strouhal number are seen in the global wavelet power spectra, roughly similar to that of a Fourier power spectrum.

It is well known from previous studies that the flow over a cylinder with tripping rods, in which reduction of fluid forces is the greatest, is qualitatively and sometimes quantitatively similar to the natural critical flow (twin-bubble flow) over a plain cylinder (Fage and Warsap, 1929). Thus, as the Reynolds number of the flow over a cylinder with tripping rods is decreased, the flow changes from a critical flow to a subcritical flow; that is, there is a threshold Reynolds number (transition Reynolds number) above which fluid forces are reduced. At Reynolds numbers below the threshold Reynolds number, fluid forces and the Strouhal number are identical with those of a plain cylinder (Fage and Warsap, 1929; James and Truong, 1972; Igarashi, 1986). The threshold Reynolds number depends on the location and diameter of tripping rods. Previous studies have shown that the threshold Reynolds numbers are 7.7×10^4 for $d/D = 0.3\%$ at $\alpha = 65^\circ$ (Fage and Warsap, 1929), 5×10^4 for $d/D = 2.5\%$ at $\alpha = 50^\circ$ (Igarashi, 1986), 4×10^4 for $d/D = 5.9\%$ at $\alpha = 40^\circ$ (Pearcey et al., 1982), and 3×10^4 for $d/D = 6.3\%$ at $\alpha = 35^\circ$ (James and Truong, 1972). In order to identify the threshold Reynolds number in the present study, Strouhal numbers were measured with decrease in the Reynolds number, and the results are presented in Fig. 12 which shows that the Strouhal number is constant throughout the range

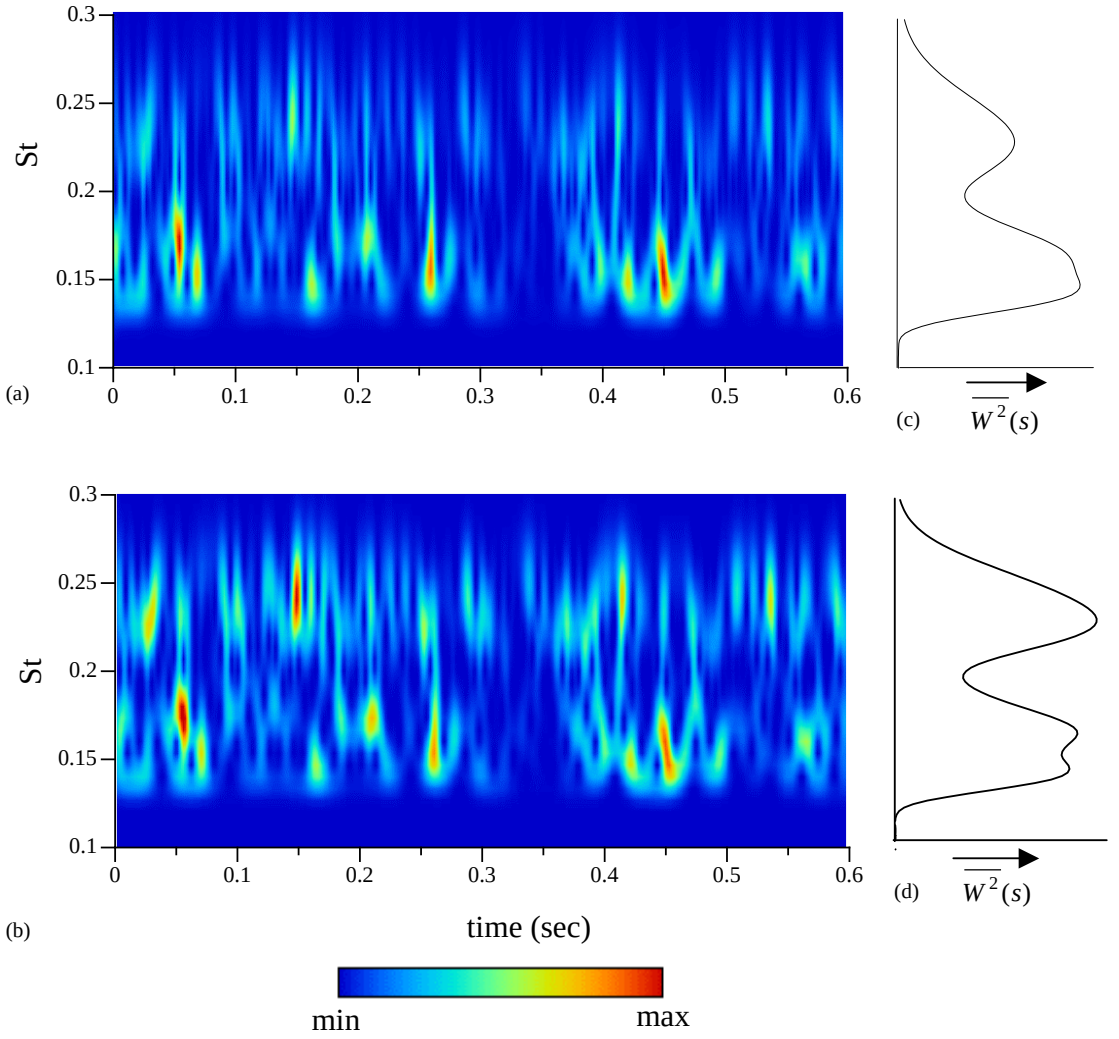

Fig. 11. (a) Wavelet power spectrum of fluctuating lifts ($d = 5$ mm, $\alpha = 42°$) with $\omega_0 = 6, p(s) = s^{-0.5}$; (b) same as (a) but for $p(s) = s^{-1.5}$; (c), (d) global wavelet power spectra for (a) and (b), respectively.

of $\mathrm{Re} = 7 \times 10^3$–$6.5 \times 10^4$, suggesting that the threshold Reynolds number was much lower than 7×10^3. However, measurement of Reynolds numbers lower than 7×10^3 was not possible using our experimental facilities.

3.2. *Tripping rods on two side-by-side cylinders*

3.2.1. *Reduction of fluid forces*

Reduction of fluid forces acting on two cylinders in a side-by-side arrangement with tripping rods on both cylinders was examined. The diameter of each tripping rod was 5 mm, and tripping rods were placed at an angle of 30° with $\delta = 0.4$ mm. Fig. 13 shows the effect of tripping rods on drag coefficient, C_D, for two cylinders in a side-by-side arrangement. The figure also includes data for plain cylinders (without tripping rods) for comparison. Since Alam et al. (2003a) has described in detail the flow characteristics, switching phenomena and characteristics of fluid forces acting on two plain cylinders in side-by-side arrangements, the data for the case of plain cylinders will be explained briefly.

In the bistable regime, in which fluid forces were found to be switched, fluid forces were decomposed for modes 'NW' and 'WW' by using a conditional sampling technique on digitally stored data. The process of decomposition has been described in detail by Alam et al. (2003a). A bistable flow appears in the range of $T/D = 0.10 \sim 1.50$ and 0.10–1.0 for plain cylinders and cylinders with tripping rods, respectively. The use of tripping rods significantly reduces drag forces

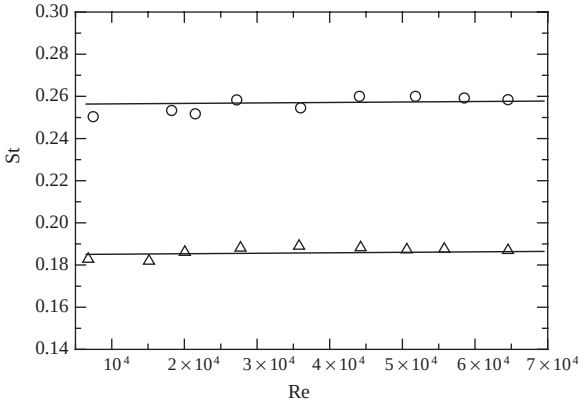

Fig. 12. Variation in Strouhal number, St, as a function of Reynolds number: △, plain cylinder; ○, cylinder with tripping rods: $d = 5$ mm, $\alpha = 30^\circ$.

acting on the cylinders. The average reduction of C_D for $T/D > 1$ is about 70%. However, the reduction of C_D at $T/D = 0.10$ is very small.

The variation in lift coefficient, C_L, as a function of spacing ratio is shown in Fig. 14. In this study, repulsive force was regarded as a positive force and attractive force was regarded as a negative force. The figure shows that the trend of C_L distribution of the plain cylinder case is similar to that of the cylinders with tripping rods. The difference between C_L values for modes 'WW' and 'NW' is large at $T/D = 0.10$ for cylinders with and without tripping rods. At this spacing, mode 'NW' causes a negative lift in both cases. Alam et al. (2003a) reported that the gap flow in the case of two plain cylinders at $T/D = 0.10$ was greatly biased toward one side and that the cylinder toward which gap flow was biased was subjected to a negative lift. Their results of flow visualization and pressure distribution also showed a greatly biased gap flow. We now examine the C_P distribution for the case of cylinders with tripping rods to obtain an understanding about negative lift at $T/D = 0.10$. Fig. 15 shows the C_P distributions for modes 'NW' and 'WW' at $T/D = 0.10$. The figure clearly shows that, in the case of mode 'NW', the high negative pressure induced by the gap flow at $\theta = 180^\circ - 280^\circ$ and the relatively high pressure at $\theta = 40^\circ - 180^\circ$ results in a negative value of C_L. The figure also shows that the stagnation point shifts near the positions of inner tripping rods, $\theta = 330^\circ$ (i.e., -30°); as a result, the inner tripping rods are ineffective and the outer tripping rods are now 60° from the stagnation point. The small pressure recovery in the range of $\theta = 10^\circ - 20^\circ$ (Fig. 15) is similar to the pressure recovery at $\theta = 40^\circ - 50^\circ$ for $\alpha = 60^\circ$ (Fig. 8(a)). Consequently, the outer tripping rods behave like those for $\alpha = 60^\circ$ (pattern B) on a single cylinder. That is the reason why the fluid forces are not reduced at $T/D = 0.10$. It is interesting to note that the angular distance between the start of pressure recovery (minimum pressure) and the stagnation point is 40° in Fig. 8(a), and the angular distance between those points is also 40° ($= 30^\circ + 10^\circ$) in Fig. 15. Thus, the outer boundary layers can be expected to separate at a point between 10° and 20°, about 15° upstream of the tripping rods. In case of the two plain cylinders, it was found that outer boundary layers separated at about $\theta = 60^\circ$.

The distributions of fluctuating drag coefficients and fluctuating lift coefficients for two plain cylinders and cylinders with tripping rods are shown in Fig. 16. It can be seen that fluctuating drag and lift are very small at and near $T/D = 0.50$. The values of C_{Df} and C_{Lf} are reduced considerably when tripping rods are used. On average, reduction of C_{Df} and that of C_{Lf} are about 62% and 88%, respectively, for $T/D > 1$. Fig. 17 shows the distribution of fluctuating pressure coefficients for $T/D = 0.10$. The distributions for modes 'NW' and 'WW' are very different. The peaks at $\theta = 265^\circ$ and 190° in modes 'WW' and 'NW', respectively, indicate the separation positions of gap flow from the cylinders (Batham, 1973; Alam et al., 2003b). In the case of mode 'NW', C_{Pf} is high in the base region, toward which the gap flow deflects.

3.2.2. Strouhal number

The distributions of Strouhal numbers, obtained from the results of Fourier spectral analysis of fluctuating lift force and fluctuating velocity measured by using hot wire probes, are shown in Fig. 18. The hotwires were positioned just $1D$ outside and $2.5D$ downstream from the centers of the cylinders (Fig. 1(a)). In our experiment, as the gap flow switched spontaneously from a side to the other, resulting in mutual change of the modes 'NW' and 'WW', the hotwires were placed symmetrically at a position where they can capture signals of vortex shedding of the both modes (Spivack, 1946). The distribution of Strouhal numbers in the case of cylinders with tripping rods is similar to that in the case of plain

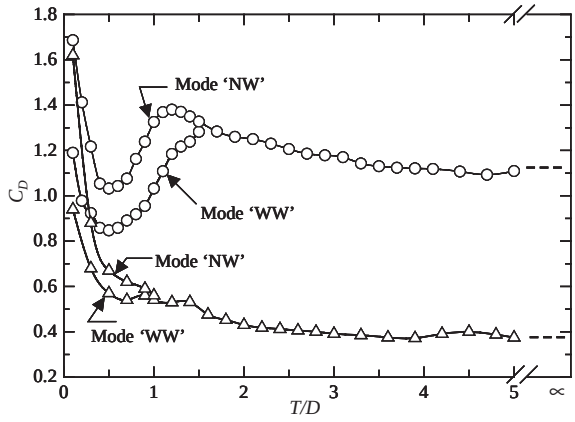

Fig. 13. Drag coefficient, C_D: ○, plain cylinders; △, cylinders with tripping rods.

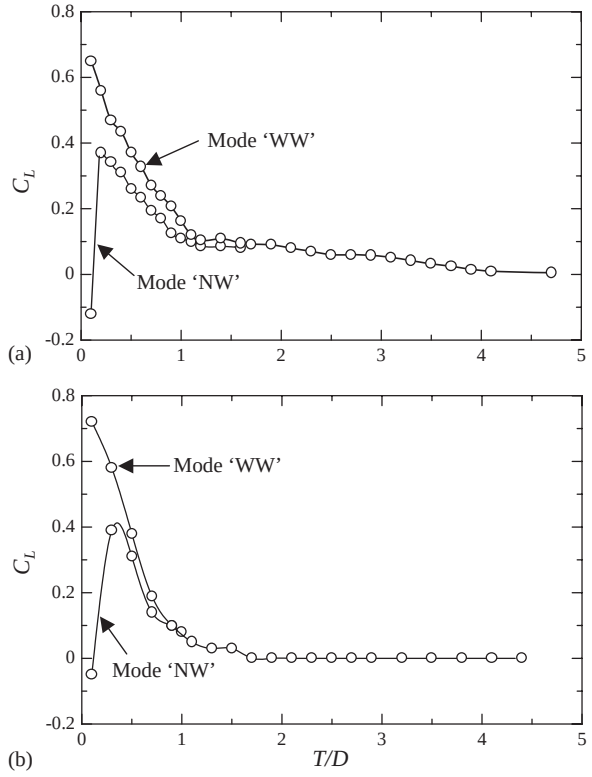

Fig. 14. Lift coefficient, C_L: (a) plain cylinders, (b) cylinders with tripping rods.

cylinders. The trends in changes in Strouhal numbers that have been indicated as high-frequency mode and low-frequency mode are well known from previous studies on two plain cylinders (Spivack, 1946; Bearman and Wadcock, 1973; Kamemoto, 1976; Kiya et al., 1980; Kim and Durbin, 1988). However, as can be seen in Fig. 18, we found another set of Strouhal numbers that has been indicated as intermediate-frequency mode. The flow pattern that is formed at $T/D > 0.90$ appears intermittently at $T/D = 0.9-0.3$, resulting in an intermediate Strouhal number whose values are the same as those as for $T/D > 0.9$. The appearance of an intermediate-frequency mode in the case of plain cylinders was also found and discussed in detail on the basis of results of modal analysis and wavelet analysis by Alam et al. (2003a).

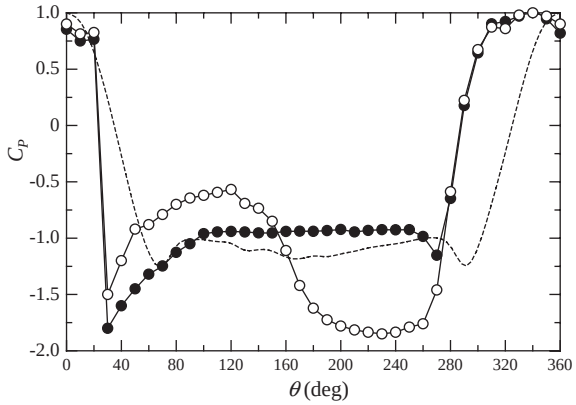

Fig. 15. Pressure coefficient, C_P, distribution for cylinders with tripping rods ($T/D = 0.10$): ○, mode 'NW'; ●, mode 'WW'; ----, single cylinder.

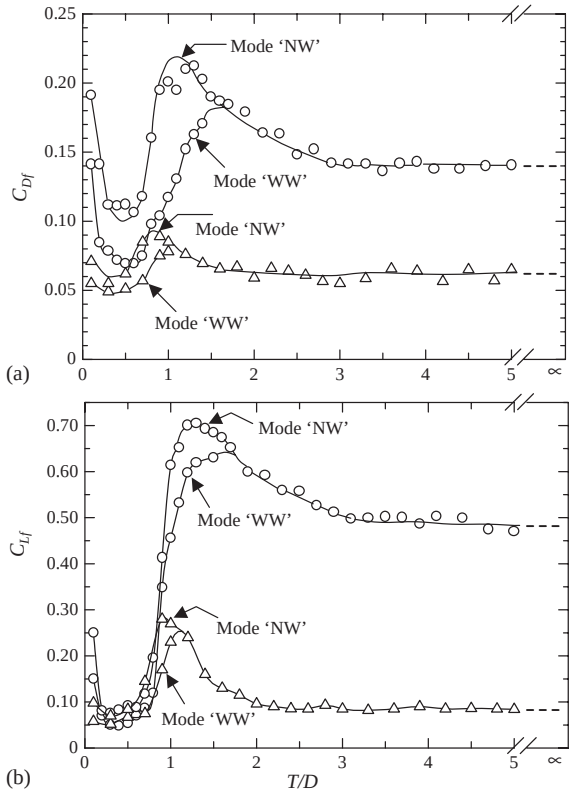

Fig. 16. Fluctuating fluid force coefficients: (a) fluctuating drag coefficient, C_{Df}, (b) fluctuating lift coefficient, C_{Lf}: ○, plain cylinder; △, cylinders with tripping rods, ----, single cylinder.

3.3. Tripping rods on two tandem cylinders

3.3.1. Reduction of fluid forces

Fluid forces acting on two cylinders in a tandem arrangement were reduced by using tripping rods on the both cylinders. Measurements of C_D, C_{Df} and C_{Lf} of two plain cylinders and two cylinders with tripping rods are shown in Fig. 19. The use of tripping rods significantly decreases the values of C_D, C_{Df} and C_{Lf} of the cylinders over the range of

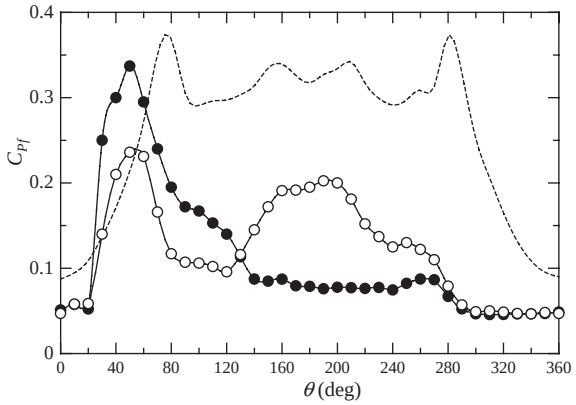

Fig. 17. Fluctuating pressure coefficient, C_{Pf}, distributions for cylinders with tripping rods ($T/D = 0.10$): ○, mode 'NW'; ●, mode 'WW'; ----, single cylinder.

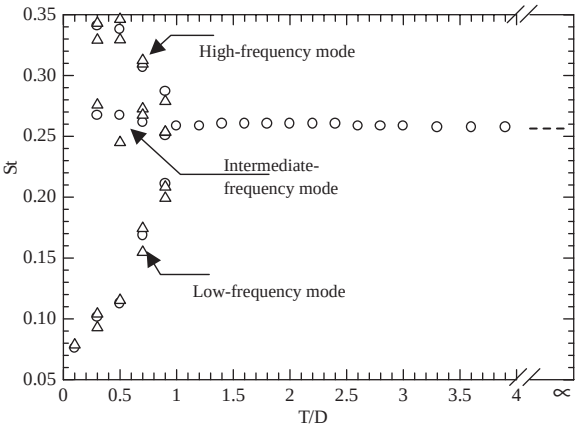

Fig. 18. Strouhal number distribution for the case of cylinders with tripping rods: ○, fluctuating lift; △, hotwire; ---- single cylinder.

spacings examined. On average, the values of C_D, C_{Df} and C_{Lf} of the upstream cylinder are reduced by 70%, 65% and 89%, respectively, for $L/D > 3$. In the case of plain cylinders, the spacing $L/D = 3.0$ at which the values of C_D, C_{Df} and C_{Lf} jump from a low value to a high value is known as the critical spacing or the bistable flow spacing (Zdravkovich, 1977; Okajima, 1979; Alam et al., 2003b). At the critical spacing, two flow patterns, namely, reattachment flow and jump flow (two vortex streets flow) appear intermittently. The reattachment flow corresponds to the lower values of C_D, C_{Df} and C_{Lf}, and the jump flow corresponds to the higher values of C_D, C_{Df} and C_{Lf}. It is interesting that the values of C_D, C_{Df} and C_{Lf} of the upstream cylinder are constant regardless of spacing when tripping rods are used on the surface of cylinders; however, there are small jumps in the values of C_D, C_{Df} and C_{Lf} of the downstream cylinder at $L/D = 2.6$. As shown in Fig. 19(a) and (b), for the downstream cylinder, the difference between coefficients associated with reattachment flow and jump flow is very small when tripping rods are used, while the difference between the values of C_{Lf} shown in Fig. 19(c) is somewhat large but smaller than that in the case of plain cylinders. Therefore, it can be concluded that action of the bistable flow is completely reduced for the upstream cylinder, and that the action of the bistable flow is reduced for the downstream cylinder. Our results for two plain cylinders agree with those obtained by Biermann and Herrnstein (1933), Zdravkovich and Pridden (1977), and Igarashi (1981).

Fig. 20 shows the distributions of C_{Pf} values for the downstream cylinder with and without tripping rods at $L/D = 3.50$. In the case of plain cylinders, the peaks at $\theta = 40^\circ$ and 320° are due to the buffeting by incoming vortices from the upstream cylinder (Alam et al., 2003b). The distribution of C_{Pf} values in the case of cylinders with tripping rods is similar to that of the plain cylinder; however, C_{Pf} is comparatively low over the whole surface except near the tripping rod positions.

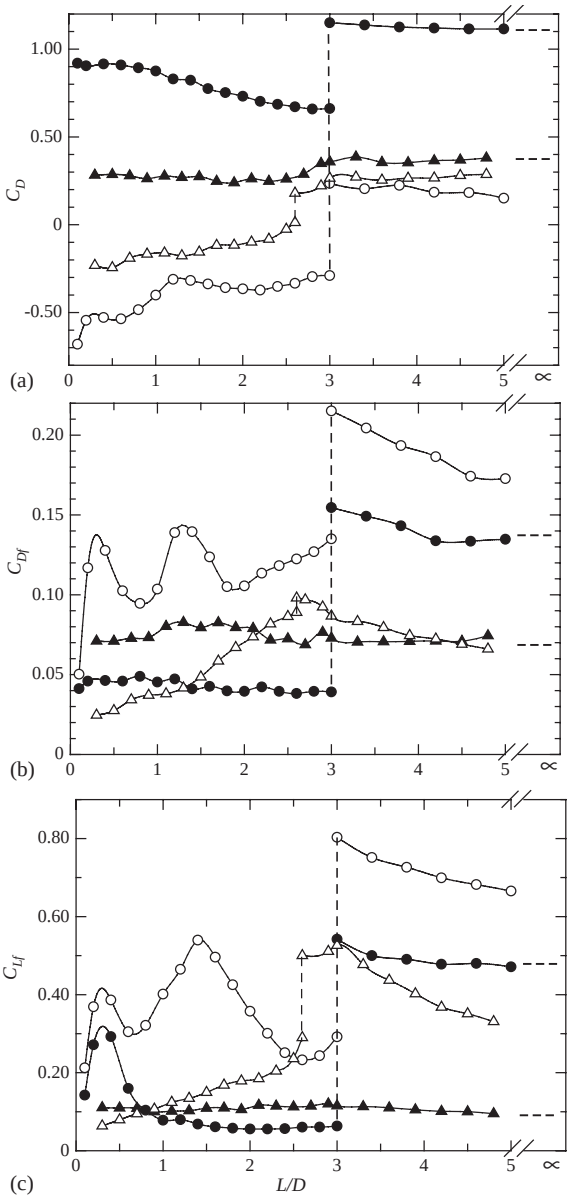

Fig. 19. Fluid forces coefficients of two cylinders in tandem arrangement: (a) C_D, (b) C_{Df}, (c) C_{Lf}: ●, upstream cylinder without tripping rods; ○, downstream cylinder without tripping rods; ▲, upstream cylinder with tripping rods; △, downstream cylinder with tripping rods.

3.3.2. Strouhal number

Strouhal numbers of the two cylinders were calculated from Fourier spectral analysis of the fluctuating lift force acting on the cylinders, and the results are shown in Fig. 21. In the case of plain cylinders, there was no distinct frequency in the power spectrum of the fluctuating lift of the upstream cylinder in the range of $L/D = 2-3$. This is due to fact that the shear layer that separated from the upstream cylinder reattached steadily onto the downstream cylinder (Alam et al., 2003b). The trend in Strouhal numbers is similar to the trends reported by Igarashi (1981) and Alam et al. (2003b). In the case of cylinders with tripping rods also, a distinct frequency in the power spectrum of the fluctuating lift of the upstream cylinder was not found in the range $L/D < 2.6$. Fig. 21 shows that jumps in the Strouhal number occur at the same spacing where fluid forces increase suddenly (Fig. 19). At the jump spacing (critical spacing), two frequencies are seen for the downstream cylinder. The lower Strouhal number corresponds to the reattachment flow,

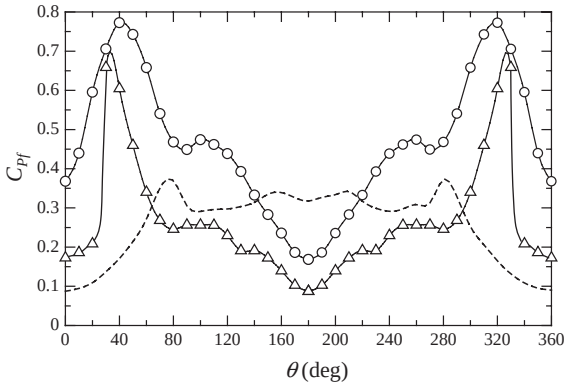

Fig. 20. Fluctuating pressure coefficient, C_{Pf}, distributions for the downstream cylinder ($L/D = 3.5$): ○, plain cylinder; △, with tripping rods; ----, single cylinder.

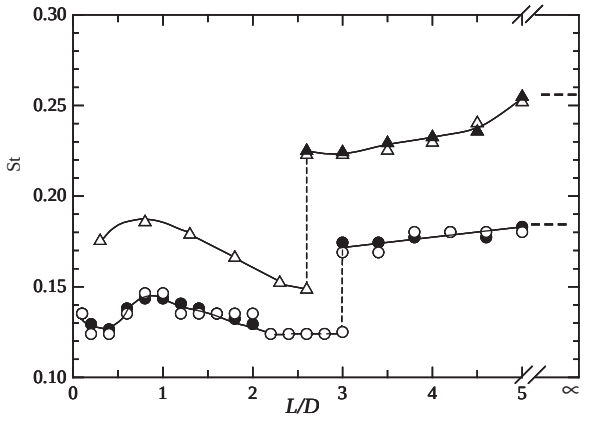

Fig. 21. Strouhal number: ●, upstream cylinder without tripping rods; ○, downstream cylinder without tripping rods; ▲, upstream cylinder with tripping rods; △, downstream cylinder with tripping rods.

and the higher Strouhal number corresponds to the jump flow. These two flow patterns spontaneously switched from one to the other at $L/D = 3$ and 2.6 for the plain cylinders and the cylinders with tripping rods, respectively.

The intermittent appearance and switching of these flow patterns can be studied by wavelet analysis. The wavelet power spectra of fluctuating lift of the downstream cylinder (without tripping rods) and global wavelet power spectra are shown in Fig. 22. It has been shown in Figs. 19(c) and 21 that the lower Strouhal number corresponds to the lower fluctuation in lift force and that the higher Strouhal number corresponds to the higher fluctuation in lift force of the downstream cylinder at the critical spacing. Hence, to highlight the energy at the lower Strouhal number (higher scale), the weighting function was chosen as $p(s) = s^{0.5}$ (Eq. (1)). For Fig. 22(a), a wave number of $\omega_0 = 6$ in the Morlet wavelet was used; this is usually chosen as the value. The figure shows the existence of two flow patterns that are associated with two Strouhal numbers of about 0.12 and 0.17, the same values as those for $L/D = 3.0$ in Fig. 21. It can be seen in Fig. 22(a) that the Strouhal number switches discontinuously from one value to the other. The wavelet power spectra as well as peaks in the global wavelet power spectra are broad-banded in the Strouhal number axis (Fig. 22(a) and (c)). However, a narrow band wavelet power spectrum can be obtained by increasing ω_0 in the Morlet wavelet. The effect of increasing ω_0 can be seen in Fig. 22(b) and (d). Fig. 22(b) and (d) is the same as Fig. 22(a) and (c) except for $\omega_0 = 12$. In Fig. 22(b) and (d), the wavelet power spectra and the peaks in the global wavelet power spectrum are comparatively narrow-banded in the Strouhal number axis, and the wavelet power spectra has been smoothened (broadened) in the time axis. From Fig. 22(b) and (d), it is easy to identify the dominant frequency (Strouhal number) of the signal, but power has been overlapped in the time axis. Hence, a larger wave number, ω_0, in the Morlet wavelet can be used when frequency resolution is more important than time resolution.

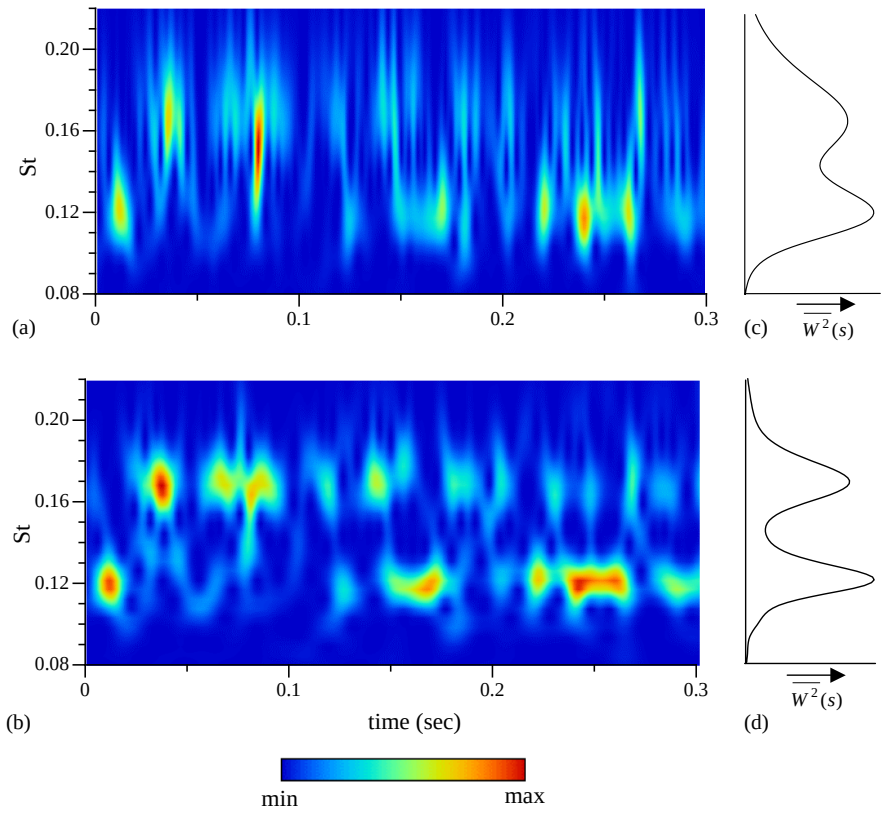

Fig. 22. (a) Wavelet power spectrum of fluctuating lifts of downstream cylinder (plain cylinders, $L/D = 3$), with $\omega_0 = 6, p(s) = s^{0.5}$; (b) same as (a) but for $\omega_0 = 12$; (c), (d) global wavelet power spectra for (a) and (b), respectively.

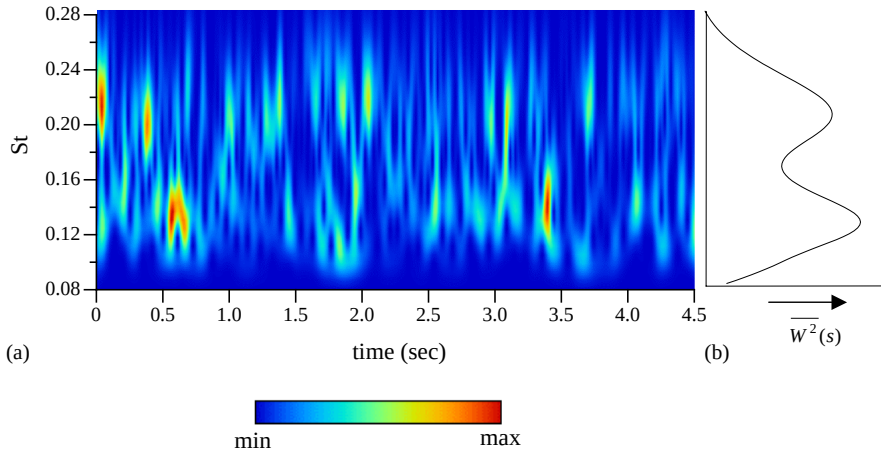

Fig. 23. (a) Wavelet power spectrum of fluctuating lifts of downstream cylinder (with tripping rods, $L/D = 2.6$) with $\omega_0 = 6, p(s) = s^{0.5}$; (b) global wavelet power spectrum.

Similarly, in the case of cylinders with tripping rods at $L/D = 2.6$ (bistable flow spacing), a wavelet power spectrum of the fluctuating lift of the downstream cylinder is shown in Fig. 23. Here also, intermittent switching of the Strouhal number from higher to lower and from lower to higher confirms the appearance of a bistable flow.

4. Conclusions

Reduction of fluid forces acting on a single cylinder and two cylinders in side-by-side and tandem arrangements was examined at a Reynolds number of 5.5×10^4. Tripping rods were used to reduce fluid forces on the cylinders. The main results of the present study are summarized as follows.

In the case of a single cylinder, the optimum angular position of tripping rods of 5 mm in diameter was found to be 30°. At this angular position of the tripping rods, C_D, C_{Df} and C_{Lf} were reduced by 67%, 61% and 87%, respectively. Three different flow patterns on the single cylinder were found when the angular position of the tripping rods was varied in the range of 20°–60°. One flow was reattachment flow ($\alpha = 20^\circ - 40^\circ$, pattern A) in which the boundary layers that separated from the tripping rods reattached on the cylinder surface behind the tripping rods, and finally laminar separation occurred from the cylinder surface. In this range of α, the fluid forces acting on the cylinder were reduced significantly and the Strouhal numbers were higher than that of the plain cylinder. Another flow pattern was separated flow ($\alpha = 45^\circ - 60^\circ$, pattern B) in which the boundary layers separated from the cylinder surface at a position sufficiently upstream of the tripping rods, and the tripping rods forced the separated boundary layer to deflect outwards, causing a stronger vortex behind the cylinder. The third flow pattern was bistable flow ($\alpha = 41^\circ - 44^\circ$, pattern C) in which flow patterns A and B intermittently appeared and switched from one to the other. The intermittent appearance of the flow patterns was confirmed by the results of wavelet analysis also.

A significant reduction in C_D, C_{Df} and C_{Lf} of two side-by-side cylinders was observed when tripping rods were used. For $T/D = 0.10$, a negative lift force acting on a cylinder associated with mode 'NW' was found in the case of two plain cylinders in side-by-side arrangement and in the case of two cylinders with tripping rods in side-by-side arrangement.

The use of tripping rods in the case of two tandem cylinders was effective in reducing the action of the bistable flow. Fluid forces acting on the upstream cylinder were almost constant regardless of spacing. Wavelet analysis is an effective tool for analyzing the switching phenomenon in the bistable flow regime.

References

Alam, M.M., Moriya, M., Takai, K., Sakamoto, H., 2002. Suppression of fluid forces acting on two square cylinders in a tandem arrangement by passive control of flow. Journal of Fluids and Structures 16, 1073–1092.

Alam, M.M., Moriya, M., Sakamoto, H., 2003a. Aerodynamic characteristics of two side-by-side circular cylinders and application of wavelet in switching phenomenon. Journal of Fluids and Structures, in this volume, doi:10.1016/j.jfluidstructs.2003.07.005.

Alam, M.M., Moriya, M., Takai, K., Sakamoto, H., 2003b. Fluctuating fluid forces acting on two circular cylinders in a tandem arrangement at a subcritical Reynolds number. Journal of Wind Engineering and Industrial Aerodynamics 91, 139–154.

Arneodo, A., Gresseau, G., Holschneider, M., 1988. Wavelet transform of multifractals. Physical Review Letters 61, 2281–2284.

Batham, J.P., 1973. Pressure distribution on circular cylinders at critical Reynolds numbers. Journal of Fluid Mechanics 57, 209–228.

Bearman, P.W., 1969. On vortex shedding from a circular cylinder in the critical Reynolds number regime. Journal of Fluid Mechanics 37, 577–585.

Bearman, P.W., Wadcock, A.J., 1973. The interaction between a pair of circular cylinder normal to a stream. Journal of Fluid Mechanics 61, 499–511.

Biermann, D., Herrnstein, J.R., 1933. The interference between struts in various combinations. National Advisory Committee for Aeronautics, Technical Report No. 468.

Chen, S.S., 1986. A review of flow-induced vibration of two circular cylinders in crossflow. Journal of Pressure Vessel Technology 108, 382–393.

Fage, A., Warsap, J.H., 1929. The effects of turbulence and surface roughness on the drag of a circular cylinder. Aeronautical Research Council, Reports and Memoranda No. 1283, pp. 1–14.

Farge, M., 1992. Wavelet transforms and their applications to turbulence. Annual Review of Fluid Mechanics 24, 395–457.

Hamdan, M.N., Jubran, B.A., Shabaneh, N.H., Abu-Samak, M., 1996. Comparison of various basic wavelets for the analysis of flow-induced vibration of a cylinder in cross-flow. Journal of Fluids and Structures 10, 633–651.

Hori, E., 1959. Experiments on flow around a pair of parallel circular cylinders. Proceedings of the 9th Japan National Congress for Applied Mechanics. Paper III-11, 231–234.

Hover, F.S., Tvedt, H., Triantafyllou, M.S., 2001. Vortex-induced vibrations of a cylinder with tripping wires. Journal of Fluid Mechanics 448, 175–195.

Igarashi, T., 1981. Characteristics of the flow around two circular cylinders arranged in tandem, (1st Report). Bulletin of the Japan Society of Mechanical Engineers 24, 323–331.

Igarashi, T., 1984. Characteristics of the flow around two circular cylinders arranged in tandem, (2nd Report). Bulletin of the Japan Society of Mechanical Engineers 27, 2380–2387.

Igarashi, T., 1986. Effect of tripping wires on the flow around a circular cylinder normal to an airstream. Bulletin of the Japan Society of Mechanical Engineers 29, 2917–2924.

James, D.F., Truong, Q.T., 1972. Wind load on a cylinder with a spanwise protrusion. Journal of the Engineering Mechanics Division, Proceedings of the American Society of Civil Engineers 98, 1573–1589.

Jendrzejczyk, J.A., Chen, S.S., 1982. Fluid forces on two circular cylinders in liquid cross-flow. In: Flow-Induced Vibration of Circular Cylindrical Structure, ASME PVP, Vol. 63, pp. 31–44.

Jendrzejczyk, J.A., Chen, S.S., 1986. Fluid forces on two circular cylinders in crossflow. In: Flow-Induced Vibration 1986, ASME PVP, Vol. 104, pp. 1–13.

Kamemoto, K., 1976. Formation and interaction of two parallel vortex streets. Bulletin of the Japan Society of Mechanical Engineers 19, 283–290.

Kareem, A., Cheng, C.M., 1999. Pressure and force fluctuations on isolated roughened circular cylinders of finite height in boundary layer flow. Journal of Fluids and Structures 13, 907–933.

Kareem, A., Kijewski, T., Lu, P.C., 1998. Investigation of interference effects for a group of finite cylinders. Journal of Wind Engineering and Industrial Aerodynamics 77 & 78, 503–520.

Kim, H.J., Durbin, P.A., 1988. Investigation of the flow between a pair of circular cylinders in the flopping regime. Journal of Fluid Mechanics 196, 431–448.

Kiya, M., Arie, M., Tamura, H., Mori, H., 1980. Vortex shedding from two circular cylinders in staggered arrangement. Journal of Fluids Engineering 102, 166–173.

Lesage, F., Gartshore, I.S., 1987. A method of reducing drag and fluctuating side force on bluff bodies. Journal of Wind Engineering and Industrial Aerodynamics 25, 229–245.

Lewalle, J., 1994. Wavelet analysis of experimental data: some methods and the underlying Physics. AIAA Journal 94, 2281–2288.

Mahir, N., Rockwell, D., 1996. Vortex formation from a forced system of two cylinders, Part II: side-by-side arrangement. Journal of Fluids and Structures 10, 491–550.

Mueller, T.J., 1961. On separation, reattachment and redevelopment of turbulent boundary-layers. Ph.D. Thesis, University of Illinois, Urbana.

Naumann, A., Quadflieg, H., 1972. Vortex generation on cylindrical buildings and its simulation in wind tunnels. In: Naudascher, E. (Ed.), Proceedings of the Flow Induced Structural Vibrations IUTAM/IAHR Symposium. Karlsruhe, Springer, pp. 730–747.

Nebres, J., Batill, S., 1993. Flow about a circular cylinder with a single large-scale surface perturbation. Experiments in Fluids 15, 369–379.

Okajima, A., 1979. Flow around two tandem circular cylinders at very high Reynolds numbers. Bulletin of the Japan Society of Mechanical Engineers 22, 504–511.

Pearcey, H.H., Cash, R.F., Salter, I.J., 1982. Flow past circular cylinders: simulation of full-scale flows at model scale. National Maritime Institute, NMI Report 131, 1–54.

Pohlhausen, K., 1921. On approximate Integration of boundary layer differential equation. Zeitschrift für Angewandte Mathenatik und Mechanik 1, 252–268 (in German).

Romberg, O., Popp, K., 1998. The influence of trip-wires on the fluid-damping-controlled instability of a flexible tube in a bundle. Journal of Fluids and Structures 12, 17–32.

Sakamoto, H., Haniu, H., Obata, .Y., Matubara, S., 1994. Optimum suppression of fluid forces acting on a circular cylinder and its effectiveness. JSME International Journal, Series B 37, 369–376.

Spivack, H.M., 1946. Vortex frequency and flow pattern in the wake of two parallel cylinders at varied spacing normal to an air stream. Journal of the Aeronautical Sciences 13, 289–301.

Szepessy, S., Bearman, P.W., 1992. Aspect ratio and end plate effects on vortex shedding from a circular cylinder. Journal of Fluid Mechanics 234, 191–217.

Torrence, C., Compo, G., 1998. A practical guide to wavelet analysis. Bulletin of the American Meteorological Society 79, 61–78.

West, G.S., Apelt, C.J., 1997. Fluctuating lift and drag forces on finite lengths of a circular cylinder in the subcritical Reynolds number range. Journal of Fluids and Structures 11, 135–158.

Zdravkovich, M.M., 1977. Review of flow interference between two circular cylinders in various arrangement. Journal of Fluids Engineering 199, 618–633.

Zdravkovich, M.M., 1981. Review and classification of various aerodynamic and hydrodynamic means for suppressing vortex shedding. Journal of Wind Engineering and Industrial Aerodynamics 7, 145–189.

Zdravkovich, M.M., 1988. Review of interference-induced oscillations in flow past two parallel circular cylinders in various arrangements. Journal of Wind Engineering and Industrial Aerodynamics 28, 183–200.

Zdravkovich, M.M., Pridden, D.L., 1977. Interference between two circular cylinders; series of unexpected discontinuities. Journal of Industrial Aerodynamics 2, 255–270.

Zhang, H., Melbourne, W.H., 1992. Interference between two circular cylinders in tandem in turbulent flow. Journal of Wind Engineering and Industrial Aerodynamics 41, 589–600.

Zhou, Y., Wang, Z.J., So, R.M.C., Xu, S.J., Jin, W., 2001. Free vibrations of two side-by-side cylinders in a cross-flow. Journal of Fluid Mechanics 443, 197–229.